

# Direct Kinetics Study of the Temperature Dependence of the CH<sub>2</sub>O Branching Channel for the CH<sub>3</sub>O<sub>2</sub> + HO<sub>2</sub> Reaction

MATTHEW J. ELROD, DANA L. RANSCHAERT, NICHOLAS J. SCHNEIDER

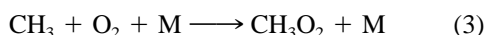
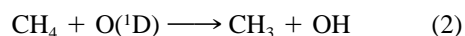
Department of Chemistry, Hope College, Holland, Michigan, 49423

Received 8 September 2000; accepted 26 January 2001

**ABSTRACT:** A direct kinetics study of the temperature dependence of the CH<sub>2</sub>O branching channel for the CH<sub>3</sub>O<sub>2</sub> + HO<sub>2</sub> reaction has been performed using the turbulent flow technique with high-pressure chemical ionization mass spectrometry for the detection of reactants and products. The temperature dependence of the CH<sub>2</sub>O-producing channel rate constant was investigated between 298 and 218 K at a pressure of 100 Torr, and the data were fitted to the following Arrhenius expression:  $1.6^{+1.0}_{-0.7} \times 10^{-15} \times \exp[(1730 \pm 130)/T]$  cm<sup>3</sup> molecule<sup>-1</sup> s<sup>-1</sup>. Using the Arrhenius expression for the overall rate of the CH<sub>3</sub>O<sub>2</sub> + HO<sub>2</sub> reaction and this result, the 298 K branching ratio for the CH<sub>2</sub>O producing channel is measured to be 0.11, and the branching ratio is calculated to increase to a value of 0.31 at 218 K, the lowest temperature accessed in this study. The results are compared to the analogous CH<sub>3</sub>O<sub>2</sub> + CH<sub>3</sub>O<sub>2</sub> reaction and the potential atmospheric ramifications of significant CH<sub>2</sub>O production from the CH<sub>3</sub>O<sub>2</sub> + HO<sub>2</sub> reaction are discussed. © 2001 John Wiley & Sons, Inc. *Int J Chem Kinet* 33: 363–376, 2001

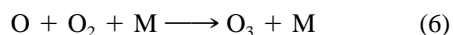
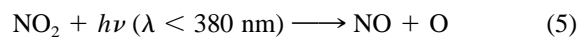
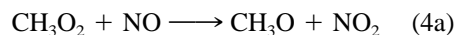
## INTRODUCTION

The methylperoxy radical (CH<sub>3</sub>O<sub>2</sub>) is an important intermediate species formed in the oxidation of methane in the atmosphere [1].

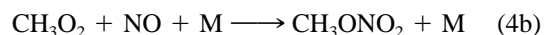


Ozone levels in the atmosphere are directly affected by CH<sub>3</sub>O<sub>2</sub> reactions, which themselves are dependent

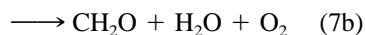
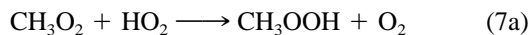
on the levels of the nitrogen oxides (NO<sub>x</sub>). Under high NO<sub>x</sub> conditions (generally, lower tropospheric conditions), CH<sub>3</sub>O<sub>2</sub> reactions lead to the production of ozone, the most deleterious constituent of photochemical smog.



CH<sub>3</sub>O<sub>2</sub> can also be temporarily removed from the ozone production cycles by the formation of reservoir species.



Correspondence to: M. J. Elrod (elrod@hope.edu)  
© 2001 John Wiley & Sons, Inc.



A potential product of reaction 4,  $\text{CH}_3\text{ONO}_2$  (from reaction 4b), has been directly measured in the atmosphere and suggested as a tracer of the photochemical age of air masses [2], but the chemical processes leading to its presence in the atmosphere remain unclear [3], despite recent attempts to establish the atmospheric significance of reaction 4b [4]. Recently, Wennberg et al. [5] reported the measurement of higher  $\text{HO}_x$  levels than predicted in the upper troposphere of the northern hemisphere, suggesting that this region of the atmosphere is more susceptible to  $\text{NO}_x$ -catalyzed ozone production than previously thought. This is an important result since it significantly impacts models that predict the effect of aviation on ozone levels in the atmosphere. Therefore, it is critical to obtain the relative rates of reaction 4 and reaction 7 and to understand the product distributions of these reactions in order to address the impact of  $\text{CH}_3\text{O}_2$  chemistry on this issue.

In the first phase of addressing these issues for  $\text{CH}_3\text{O}_2$  chemistry, we investigated reaction 4 by measuring the temperature dependence of the overall rate constant for the  $\text{CH}_3\text{O}_2 + \text{NO}$  reaction and establishing an upper limit for the  $\text{CH}_3\text{ONO}_2$ -producing branching channel [4]. This article details the second phase of this work: an investigation of the kinetics of the  $\text{CH}_3\text{O}_2 + \text{HO}_2$  reaction. The overall rate constant  $k_7$  for this reaction has received considerable previous study by flash photolysis (FP) techniques [6–13]. As the JPL recommendation for the overall rate constant for this reaction states [14], the agreement among the various studies is not very good. The lack of a consensus result for this rate constant is most likely due to the near universal use of overlapping  $\text{HO}_2$  and  $\text{CH}_3\text{O}_2$  UV absorption detection methods (for which different UV cross sections have been used in the determination of the absolute rate constants) and the complicated secondary chemistry resulting from the peroxy radical self-reactions ( $\text{CH}_3\text{O}_2 + \text{CH}_3\text{O}_2$  and  $\text{HO}_2 + \text{HO}_2$ ).

As for the  $\text{CH}_3\text{O}_2 + \text{NO}$  reaction, a secondary branching channel for the  $\text{CH}_3\text{O}_2 + \text{HO}_2$  reaction has also been proposed:



There have been several investigations of the  $\text{CH}_3\text{OOH}$ -producing rate constant  $k_{7a}$  [9,15,16] as well as one indirect investigation of the  $\text{CH}_2\text{O}$ -producing

rate constant  $k_{7b}$  (using the isotopically substituted  $\text{CD}_3\text{O}_2$  reactant and detecting the  $\text{HDO}$  product from reaction 7b) [8]. These studies are in fairly wide disagreement, with estimates for the secondary  $\text{CH}_2\text{O}$ -producing channel branching ratio [ $k_{7b}/(k_{7a} + k_{7b})$ ] ranging from as low as zero [16] to as high as 0.40 [8]. Indeed, because of this lack of agreement, the JPL recommendation for the  $\text{CH}_3\text{O}_2 + \text{HO}_2$  reaction specifically calls for new studies using direct  $\text{CH}_2\text{O}$  detection techniques [14]. Because the products  $\text{CH}_3\text{OOH}$  (from reaction 7a) and  $\text{CH}_2\text{O}$  (from reaction 7b) are characterized by quite different photochemical reactivity (with a potentially varying impact on  $\text{HO}_x$  cycling and  $\text{O}_3$  production efficiency), it is very important to quantitatively establish the atmospheric relevance of reaction 7b. In addition, it has been suggested by Ayers et al. [17] and Weller et al. [18] that the underprediction by atmospheric models (which generally assumes a zero branching ratio value for reaction (7b)) of  $\text{CH}_2\text{O}$  levels in the remote troposphere may be a consequence of a significant  $\text{CH}_2\text{O}$ -forming product channel for the  $\text{CH}_3\text{O}_2 + \text{HO}_2$  reaction.

In this article we describe our investigation of the kinetics of the  $\text{CH}_3\text{O}_2 + \text{HO}_2$  reaction conducted at pressures near 100 Torr and at a range of temperatures extending to those found in the upper troposphere using a turbulent flow (TF) tube coupled to a high-pressure chemical ionization mass spectrometer (CIMS). It has been previously shown that TF technique can be used to accurately determine the rate constants of reactions at pressures ranging from 50 to 760 Torr and at temperatures as low as 180 K [19]. As in our previous kinetics studies of the  $\text{CH}_3\text{O}_2 + \text{NO}$  and  $\text{C}_2\text{H}_5\text{O}_2 + \text{NO}$  reactions using the coupled TF-CIMS approach [4,20], we are able to directly access atmospheric pressure and temperature conditions and sensitively monitor many of the relevant reactants and products for the  $\text{CH}_3\text{O}_2 + \text{HO}_2$  reaction. In contrast to previous work on this reaction, we are able to unambiguously monitor both reactants ( $\text{CH}_3\text{O}_2$  and  $\text{HO}_2$ ) as well as a species ( $\text{CH}_3\text{OOH}$  or  $\text{CH}_2\text{O}$ ) from each of the potential product channels 7a and 7b. This capability allows for the first direct product study of reaction 7b.

## EXPERIMENTAL

### Turbulent Fast-Flow Tube Kinetics

A schematic of the experimental apparatus is presented in Figure 1 and is similar to that used in a previous study of  $\text{HO}_2 + \text{BrO}$  [21] with the  $\text{BrO}$  source

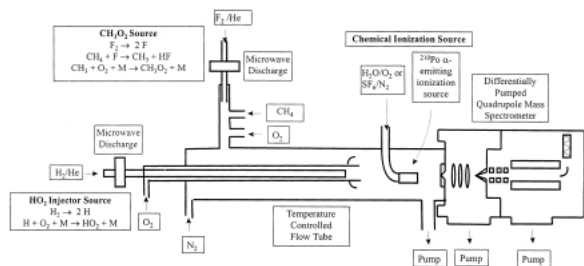
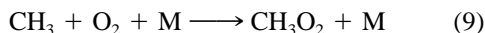
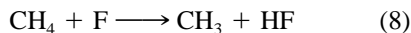


Figure 1 Experimental apparatus.

replaced by the CH<sub>3</sub>O<sub>2</sub> source described in Scholtens et al. [4] The flow tube was constructed with 2.2 cm i.d. Pyrex tubing and was 60 cm in total length. A large flow of nitrogen carrier gas (approximately 30 STP liter min<sup>-1</sup>) was injected at the rear of the flow tube. The gases necessary to generate CH<sub>3</sub>O<sub>2</sub> were introduced through a 10-cm-long, 12.5-mm diameter side-arm located at the rear of the flow tube. HO<sub>2</sub> was generated in a triple-nested movable injector. The outer encasement (made from corrugated Teflon tubing) was used so that the injector could be moved to various injector positions without breaking any vacuum seals, as well as to prevent ambient gases from condensing on cold portions of the injector. A fan-shaped Teflon device was placed at the end of the injector in order to enhance turbulent mixing. The polonium-210, alpha-emitting ionization source was placed between the temperature-regulated flow tube and the inlet to the quadrupole mass spectrometer. Most of the flow-tube gases were removed at the CIMS inlet by a 31-L s<sup>-1</sup> roughing pump. All gas flows were monitored with calibrated mass flow meters. The flow-tube pressure was measured upstream of the ionization source using a 0–1,000 Torr capacitance manometer. The temperature was determined at both the entrance and exit points of the temperature-regulated region of the flow tube using Cu–constantan thermocouples.

## Reactant Preparation

CH<sub>3</sub>O<sub>2</sub> was generated using the following reactions:



( $k_8 = 6.7 \times 10^{-11}$  cm<sup>3</sup> molecule<sup>-1</sup> s<sup>-1</sup> and  $k_9 = 4.9 \times 10^{-13}$  cm<sup>3</sup> molecule<sup>-1</sup> s<sup>-1</sup> at 100 Torr) [14]. Fluorine atoms were produced by combining a 2.0 STP liter min<sup>-1</sup> flow of helium (99.999%), which had passed through a silica gel trap immersed in liquid nitrogen,

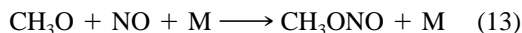
with a 0.5–5.0 STP ml min<sup>-1</sup> flow of a 1% F<sub>2</sub>/He mixture (Excimer grade), which then passed through a microwave discharge produced by a Beenakker cavity operating at 50 W. To generate CH<sub>3</sub>, the fluorine atoms were then injected into a sidearm and mixed with an excess of CH<sub>4</sub> (CP grade,  $\sim 10^{15}$  molecule cm<sup>-3</sup>) in order to ensure that no fluorine atoms were introduced into the main flow. CH<sub>3</sub>O<sub>2</sub> was then produced by the addition of an excess of O<sub>2</sub> (99.995%;  $\sim 1 \times 10^{16}$  molecule cm<sup>-3</sup>) just downstream of the production of CH<sub>3</sub>. Absolute CH<sub>3</sub>O<sub>2</sub> concentrations were determined by the titration reaction:



( $k_{10} = 7.8 \times 10^{-12}$  cm<sup>3</sup> molecule<sup>-1</sup> s<sup>-1</sup>) [14] and subsequent calibration of the NO<sub>2</sub> mass spectrometer signal. Computer modeling of these titration conditions indicates that slightly more NO<sub>2</sub> is produced than CH<sub>3</sub>O<sub>2</sub> initially present because of the following secondary reactions:



( $k_{11} = 1.9 \times 10^{-15}$  cm<sup>3</sup> molecule<sup>-1</sup> s<sup>-1</sup> and  $k_{12} = 8.2 \times 10^{-12}$  cm<sup>3</sup> molecule<sup>-1</sup> s<sup>-1</sup>) [14]. Therefore, the measured NO<sub>2</sub> concentrations must be adjusted to determine the correct [CH<sub>3</sub>O<sub>2</sub>]<sub>0</sub> value. However, for typical O<sub>2</sub> and NO concentrations, the conversion factor was close to unity ([NO<sub>2</sub>]<sub>titration</sub> = 1.08 [CH<sub>3</sub>O<sub>2</sub>]<sub>0</sub>) because the following reaction was dominant over reaction (11):



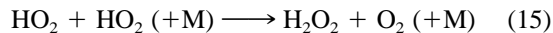
( $k_{13} = 1.3 \times 10^{-11}$  cm<sup>3</sup> molecule<sup>-1</sup> s<sup>-1</sup> at 100 Torr) [14]. Reaction 13 has a smaller branching channel to produce HNO and CH<sub>2</sub>O, but since neither of these products produces or consumes NO<sub>2</sub> under our flow reactor conditions, it is not expected to impact the titration results. NO<sub>2</sub> impurities in the NO (CP grade) used in reaction (10) were removed by the use of a dry ice/methanol-cooled silica gel trap placed between the NO reservoir (usually a 3% mixture in N<sub>2</sub>) and the flow tube. For this study, CH<sub>3</sub>O<sub>2</sub> concentrations ranged from about 3 to  $10 \times 10^{11}$  molecule cm<sup>-3</sup>.

HO<sub>2</sub> was generated from the following reaction:



( $k_{14} = 2.0 \times 10^{-13}$  cm<sup>3</sup> molecule<sup>-1</sup> s<sup>-1</sup> at 100 Torr)

[14]. Because  $\text{HO}_2$  was introduced through a movable injector where the corresponding concentrations are  $\sim 30$  times higher than in the main flow tube, the disproportionation reaction:



( $k_{15} = 1.8 \times 10^{-12} \text{ cm}^3 \text{ molecule}^{-1} \text{ s}^{-1}$  at 100 Torr) [14] is a concern in the production of large quantities of  $\text{HO}_2$ . By taking advantage of the long lifetime of H-atoms, this difficulty was surmounted by using a nested injector that kept the hydrogen atoms (entrained in the inner 3-mm alumina tube) and oxygen molecules (entrained in the outer 6-mm Pyrex tube) separate throughout all but the last 1 cm of the injector. The hydrogen atoms were allowed to mix with a very large excess of  $\text{O}_2$  ( $\sim 3 \times 10^{17} \text{ molecule cm}^{-3}$  inside the injector) for only about 1 ms, allowing reaction 14 to virtually go to completion, but preventing significant self-reaction of  $\text{HO}_2$ . Hydrogen atoms were generated by combining a 5.0 STP  $\text{L min}^{-1}$  flow of helium (99.999%, which had passed through a liquid-nitrogen-cooled silica gel trap) with a 0.5 to 4.0 STP  $\text{mL min}^{-1}$  flow of a 10%  $\text{H}_2$ (99.9%)/He mixture, which was then sent through a microwave discharge produced by a Beenaker cavity operating at 70 W. Absolute  $\text{HO}_2$  concentrations were determined in a fashion similar to that for  $\text{CH}_3\text{O}_2$ :



followed by calibration of the  $\text{NO}_2$  mass spectrometer signal.

### $\text{CH}_2\text{O}$ Branching-Channel Measurements

In these studies, the production of  $\text{CH}_2\text{O}$  from reaction (7b) was monitored directly over a reaction time of  $\sim 25$  ms. The absolute reaction times were calculated from the flow velocity and the distance between the injector and the mass spectrometer sampling aperture. Computer modeling was used to extract the rate constant  $k_{7b}$  from the observed production of  $\text{CH}_2\text{O}$  and the initial concentrations of all relevant chemical species. In order to determine the detection sensitivity of the mass spectrometer for  $\text{CH}_2\text{O}$ , two different calibration methods were employed. The first method involved the preparation of a standard sample of  $\text{CH}_2\text{O}$  and the introduction of a metered flow of  $\text{CH}_2\text{O}$  to the system. The standard  $\text{CH}_2\text{O}$  sample was prepared by heating paraformaldehyde and transferring the vapor to a carefully dried glass bulb. The  $\text{CH}_2\text{O}$  was then diluted with  $\text{N}_2$  and added to the system for direct

mass-spectrometric calibration. This procedure was somewhat troublesome in that the mass-spectrometer signal depended on the time elapsed since the sample was prepared. This effect was probably due to a drop in the gaseous  $\text{CH}_2\text{O}$  concentration as a result of the reformation of paraformaldehyde on the glass bulb walls or on the surfaces of the mass flow meter. Although a regular remixing of the  $\text{CH}_2\text{O}$  standard sample solved this problem, we choose to employ a more convenient, alternative  $\text{CH}_2\text{O}$  calibration method. This second method takes advantage of the chemistry of the  $\text{CH}_3\text{O}_2/\text{NO}$  calibration:



By using high  $\text{O}_2$  concentrations, most of the  $\text{CH}_3\text{O}_2$  reactant can be converted to  $\text{CH}_2\text{O}$ , with the result that a secondary calibration for  $\text{CH}_2\text{O}$  can be made by reference to the  $\text{NO}_2$  calibration that is part of the  $\text{CH}_3\text{O}_2$  procedure. In order to effect the most advantageous conditions, we used  $\text{O}_2$  as the carrier gas for the  $\text{CH}_3\text{O}_2/\text{NO}$  titration/calibration experiments (for experiments at 100 Torr total pressure,  $[\text{O}_2] > 3.0 \times 10^{18} \text{ molecule cm}^{-3}$ ), so that nearly all of the  $\text{CH}_3\text{O}_2$  initially present is converted to  $\text{CH}_2\text{O}$  (for typical conditions,  $[\text{CH}_2\text{O}] = 0.8[\text{CH}_3\text{O}_2]$ ). Since the  $\text{CH}_2\text{O}$  for this calibration process is generated *in situ*, the problems with paraformaldehyde formation are avoided. Therefore, the  $\text{CH}_3\text{O}_2/\text{NO}$  titration/calibration approach was routinely used for  $\text{CH}_2\text{O}$  calibration, while the direct standard sample  $\text{CH}_2\text{O}$  method was used only occasionally to ensure the consistency of the two approaches.

### Chemical Ionization Mass Spectrometric Detection

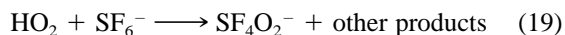
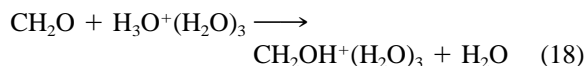
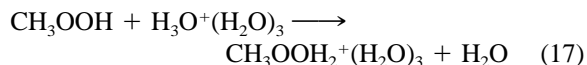
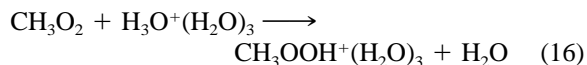
A positive ion chemical ionization scheme (with  $\text{H}_3\text{O}^+(\text{H}_2\text{O})_3$  as the reagent ion) was used to detect  $\text{CH}_3\text{O}_2$ ,  $\text{CH}_3\text{OOH}$ , and  $\text{CH}_2\text{O}$  and a negative ion chemical ionization scheme (with  $\text{SF}_6^-$  as the reagent ion) was used to detect  $\text{HO}_2$  and  $\text{NO}_2$  with the quadrupole mass spectrometer.  $\text{H}_3\text{O}^+$  was produced in the ion source by passing a large  $\text{O}_2$  flow (5 STP  $\text{L min}^{-1}$ ) through the polonium-210 alpha-emitting ionization source (with  $\text{H}_2\text{O}$  impurities being sufficiently abundant to produce sufficient quantities of reagent ions).  $\text{SF}_6^-$  was produced in the ion source by passing a large  $\text{N}_2$  flow (5 STP  $\text{L min}^{-1}$ ) and 1.0 STP  $\text{mL min}^{-1}$  of a 10 %  $\text{SF}_6/\text{N}_2$  mixture through the ionization source. The commercial ionization source consisted of a hol-

low cylindrical (length: 69 mm; diameter: 12.7 mm) aluminum body with 10 mCurie ( $3.7 \times 10^8$  disintegrations s<sup>-1</sup>) of polonium-210 coated on the interior walls.

Ions were detected with a quadrupole mass spectrometer housed in a two-stage differentially pumped vacuum chamber. Flow tube gases (neutrals and ions) were drawn into the front chamber through a 0.1-mm aperture, which was held at a potential of  $\pm 210$  V. The ions were focused by three lenses constructed from 3.8-cm i.d., 4.8-cm o.d. aluminum gaskets. The front chamber was pumped by a 6-inch, 2,400 L s<sup>-1</sup> diffusion pump. The gases entered the rear chamber through a skimmer cone with a 1.0-mm orifice (held at  $\pm 130$  V), which was placed approximately 5 cm from the front aperture. The rear chamber was pumped by a 250-L s<sup>-1</sup> turbomolecular pump. Once the ions passed through the skimmer cone, they were mass filtered and detected with a quadrupole mass spectrometer.

### Chemical Ionization Schemes

The following chemical ionization schemes were used to detect the species CH<sub>3</sub>O<sub>2</sub>, CH<sub>3</sub>OOH, CH<sub>2</sub>O, HO<sub>2</sub>, and NO<sub>2</sub>:



The rates of reactions (18) and (20) have been measured previously ( $k_{18} = 1.4 \times 10^{-9}$  cm<sup>3</sup> molecule<sup>-1</sup> s<sup>-1</sup> and  $k_{20} = 1.4 \times 10^{-10}$  cm<sup>3</sup> molecule<sup>-1</sup> s<sup>-1</sup>) [22,23], reaction (16) has been used in our previous study of the CH<sub>3</sub>O<sub>2</sub> + NO reaction [4], reaction (19) has been used in a previous study of the HO<sub>2</sub> + BrO reaction [21], and reaction (17) had been predicted to be thermodynamically feasible on the basis of electronic structure calculations [24].

For the low-temperature studies, liquid-nitrogen-cooled silicone oil was used as the coolant for the jacketed flow tube, and the nitrogen carrier gas was pre-cooled by passing it through a copper coil immersed in a liquid N<sub>2</sub> reservoir followed by resistive heating.

The temperature was controlled in the reaction region to within 1 K.

## RESULTS AND DISCUSSION

### Overview of Measurements

The use of relatively low concentrations of reactants (to minimize peroxy–peroxy self-reaction), relatively large flow velocities (necessary to ensure turbulent flow conditions) and a relatively small overall rate constant prevented the carrying out of a pseudo-first-order kinetics study of the overall rate constant. Instead, reactants and products were monitored as a function of time, and kinetics models were used to compare and/or fit the desired rate constants. The relevant reactions for kinetic modeling of the system are given in Table I. In this study, absolute concentration calibrations were obtained for CH<sub>3</sub>O<sub>2</sub> and CH<sub>2</sub>O, thus allowing direct use of the kinetics data for these species. Because of the critical importance of the accuracy of the CH<sub>2</sub>O calibration approach, a comparison of the two CH<sub>2</sub>O calibration methods is presented in Figure 2, illustrating the consistency of the two techniques.

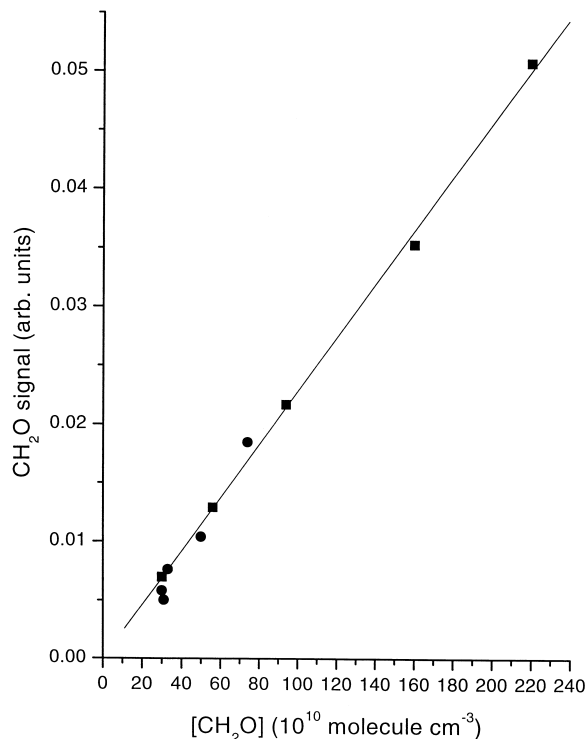


**Figure 2** Comparison of CH<sub>2</sub>O calibration methods (■: standard sample method; ●: CH<sub>3</sub>O<sub>2</sub> + NO + O<sub>2</sub> titration method).

**Table I** Kinetics Parameters for Branching Ratio Determination

Reaction <sup>a</sup>	A (cm <sup>3</sup> s <sup>-1</sup> molecule <sup>-1</sup> )	E <sub>a</sub> /R (K)
CH <sub>3</sub> O <sub>2</sub> + HO <sub>2</sub> → products	3.8 × 10 <sup>-13</sup>	-800
CH <sub>3</sub> O <sub>2</sub> + CH <sub>3</sub> O <sub>2</sub> → CH <sub>3</sub> OOCH <sub>3</sub> + O <sub>2</sub>	2.5 × 10 <sup>-13</sup> × 0.1	-190
CH <sub>3</sub> O <sub>2</sub> + CH <sub>3</sub> O <sub>2</sub> → CH <sub>3</sub> O + CH <sub>3</sub> O + O <sub>2</sub>	2.5 × 10 <sup>-13</sup> × f(T) <sup>b</sup>	-190
CH <sub>3</sub> O <sub>2</sub> + CH <sub>3</sub> O <sub>2</sub> → CH <sub>2</sub> O + CH <sub>3</sub> OH + O <sub>2</sub>	2.5 × 10 <sup>-13</sup> × (0.9 - f(T))	-190
HO <sub>2</sub> + HO <sub>2</sub> → H <sub>2</sub> O <sub>2</sub> + O <sub>2</sub>	2.3 × 10 <sup>-13</sup>	-600
HO <sub>2</sub> + HO <sub>2</sub> + M → H <sub>2</sub> O <sub>2</sub> + O <sub>2</sub> + M	1.7 × 10 <sup>-33</sup> × [M]	-1000
CH <sub>3</sub> O + O <sub>2</sub> → CH <sub>2</sub> O + HO <sub>2</sub>	3.9 × 10 <sup>-14</sup>	900
CH <sub>3</sub> O + CH <sub>3</sub> O <sub>2</sub> → CH <sub>2</sub> O + CH <sub>3</sub> OOH <sup>c</sup>	2.6 × 10 <sup>-12</sup>	0
CH <sub>3</sub> O + CH <sub>3</sub> O → CH <sub>2</sub> O + CH <sub>3</sub> OH <sup>d</sup>	1.3 × 10 <sup>-11</sup>	0
HO <sub>2</sub> + CH <sub>2</sub> O → adduct	6.7 × 10 <sup>-15</sup>	-600

<sup>a</sup>Rate constants calculated from  $k(T) = Ae^{-E_a/RT}$ . All rate constant parameters from the JPL compilation (DeMore, W. B.; Sander, S. P.; Howard, C. J.; Ravishankara, A. R.; Golden, D. M.; Kolb, C. E.; Hampson, R. F.; Kurylo, M. J.; Molina, M. J. Chemical Kinetics and Photochemical Data for Use in Stratospheric Modeling, JPL Publication 97-4; Jet Propulsion Laboratory: Pasadena, California, 1997), unless otherwise indicated.

<sup>b</sup>Temperature-dependent branching ratio calculated from  $f(T) = \left[1 + e^{\left(\frac{1131}{T} - 294\right)}\right]^{-1}$

<sup>c</sup>Rate constant parameters from Heicklen, J.; Adv Photochem 1988, 14, 177.

<sup>d</sup>Rate constant parameters from Biggs, P.; Canosa-Mas, C. E.; Fracheboud, J.-M.; Shallcross, D. E.; Wayne, R. P. J Chem Soc Faraday Trans. 1997, 93, 2481.

An approximate calibration for CH<sub>3</sub>OOH (constructed by using the same mass spectrometer sensitivity factor as was determined for CH<sub>3</sub>O<sub>2</sub>) was used in order to allow an estimate of the rate of formation of this product. Typical concentration vs. time profiles for the species CH<sub>3</sub>O<sub>2</sub> and CH<sub>3</sub>OOH are presented in Figures 3 and 4, respectively. In order to facilitate discussion of background contributions to the observed CH<sub>2</sub>O signal, the raw data (signal vs. injector distance) collected for the CH<sub>2</sub>O profiles are presented in Figure 5, and the time-dependent production of CH<sub>2</sub>O (with several different assumed values for  $k_{7b}$  overlaid) is presented in Figure 6. HO<sub>2</sub> profiles were not routinely collected because HO<sub>2</sub> concentrations were generally not significantly varied ( $\sim 1.2 \times 10^{12}$  molecule cm<sup>-3</sup>), and the decay profiles of HO<sub>2</sub> were significantly influenced by the HO<sub>2</sub> + HO<sub>2</sub> self-reaction.

### Overall Rate-Constant Evaluation

Figure 3 contains a kinetics plot ([CH<sub>3</sub>O<sub>2</sub>] vs. time) for an experiment performed at 100 Torr and 298 K (squares), as well as the predicted CH<sub>3</sub>O<sub>2</sub> decay (solid line) from a model calculation using the calibrated initial concentrations of CH<sub>3</sub>O<sub>2</sub> and HO<sub>2</sub> and the reactions listed in Table I. As the graph indicates, there is good agreement between our experimental data and modeling results that employ the JPL recommendation [14] for the overall rate constant for CH<sub>3</sub>O<sub>2</sub> + HO<sub>2</sub> (which is based on the earlier FP studies). We also find that our temperature-dependence results for

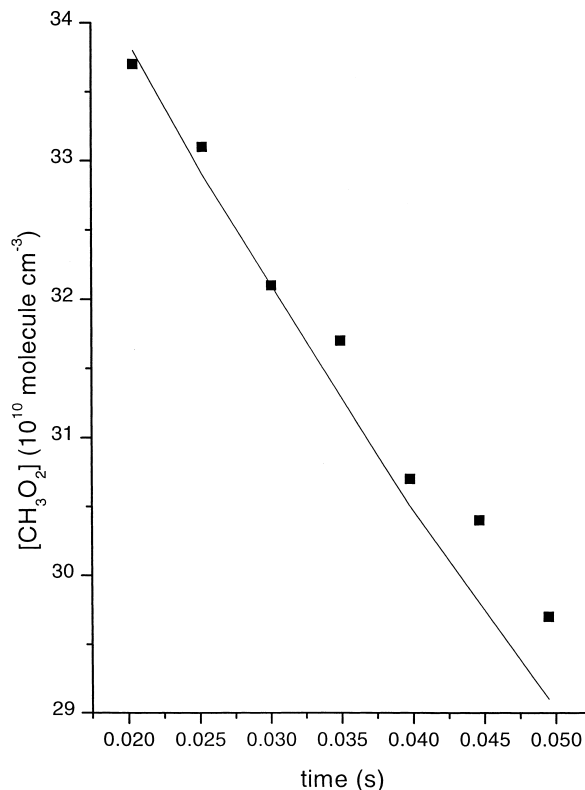


**Figure 3** [CH<sub>3</sub>O<sub>2</sub>] vs. time for the CH<sub>3</sub>O<sub>2</sub> + HO<sub>2</sub> reaction at 100 Torr, 298 K, [CH<sub>3</sub>O<sub>2</sub>]<sub>0</sub> = 3.8 × 10<sup>11</sup> molecule cm<sup>-3</sup> and [HO<sub>2</sub>]<sub>0</sub> = 1.0 × 10<sup>12</sup> molecule cm<sup>-3</sup> (■: actual data; —: model).

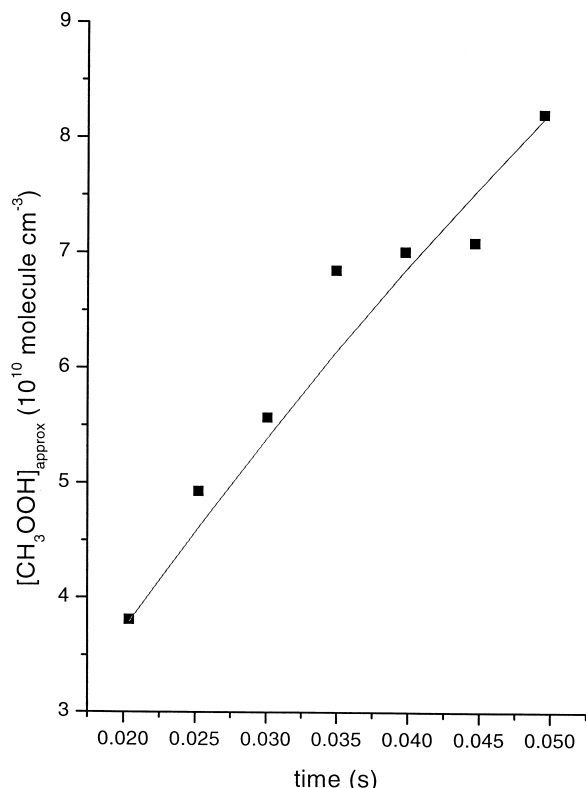


**Figure 4**  $[\text{CH}_3\text{OOH}]_{\text{approx}}$  vs. time for the  $\text{CH}_3\text{O}_2 + \text{HO}_2$  reaction at 100 Torr, 298 K,  $[\text{CH}_3\text{O}_2]_0 = 3.8 \times 10^{11} \text{ molecule cm}^{-3}$  and  $[\text{HO}_2]_0 = 1.0 \times 10^{12} \text{ molecule cm}^{-3}$  (■: actual data; —: model).

$\text{CH}_3\text{O}_2$  decay are well predicted by the same model. However, as we pointed out in the previous paragraph, experimental conditions constrain our measurements to conditions of relatively slow rates of reactant decay (the decay presented in Figure 3 represents only about a 12% loss of  $\text{CH}_3\text{O}_2$  over the reaction time accessed). Therefore, from this kinetics analysis standpoint, this first use of a fast-flow method for the  $\text{CH}_3\text{O}_2 + \text{HO}_2$  reaction is at a disadvantage compared to earlier flash-photolysis studies in which larger peroxy radical decays were observed. We estimate that our measured decays are consistent with values between a factor of 0.7 (lower bound) and 1.3 (upper bound) of the JPL recommended value (which currently indicates an estimated upper-bound uncertainty factor of 2.0 at 298 K for this reaction [14]). However, if the uncertainties in the absolute concentrations of  $\text{HO}_2$  and  $\text{CH}_3\text{O}_2$  (as well as other potential systematic uncertainties) are considered, we estimate an overall upper-bound uncertainty factor for the overall rate constant of 1.7, which is a slight improvement over the current uncertainty value. However, it is important to point out that our detection methodology is more reliable than pre-

vious studies, in that our CIMS detection and calibration methods for  $\text{CH}_3\text{O}_2$  and  $\text{HO}_2$  are completely independent of one another (in contrast to the difficult UV detection problems presented by the overlapping peroxy radical spectra in those same flash-photolysis studies). Therefore, our TF-CIMS measurements of  $\text{CH}_3\text{O}_2$  decay can be considered as complementary to the earlier flash-photolysis experiments in that, despite the fact that our fast-flow approach suffers by comparison in terms of extent of reaction observed, our chemical ionization detection technique is not hindered by the same detection complexities that plague UV detection of peroxy species.

### Branching Channel Rate-Constant Determination

Figure 4 contains a kinetics plot ( $[\text{CH}_3\text{OOH}]_{\text{approx}}$  vs. time) for an experiment performed at 100 Torr and 298 K (squares), as well as the predicted  $\text{CH}_3\text{OOH}$  rise (solid line) from a model calculation using the

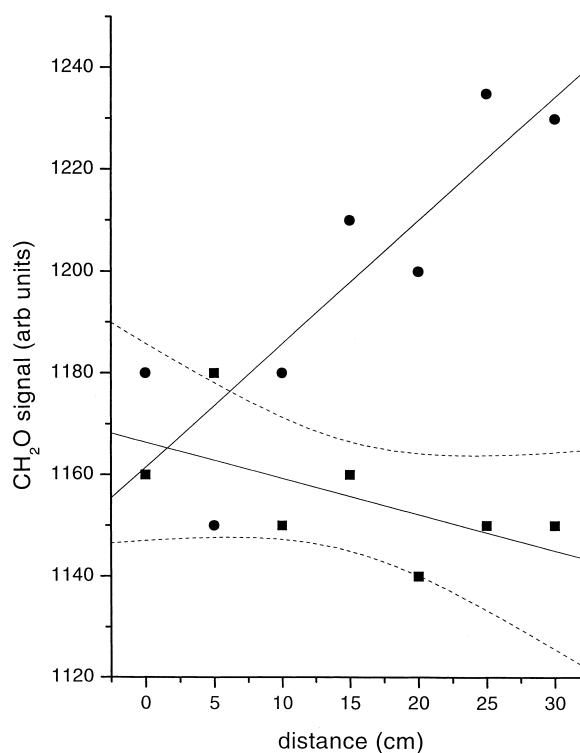


**Figure 5** Observed production of  $\text{CH}_2\text{O}$  (●) from the  $\text{CH}_3\text{O}_2 + \text{HO}_2$  reaction at 100 Torr, 298 K,  $[\text{CH}_3\text{O}_2]_0 = 6.3 \times 10^{11} \text{ molecule cm}^{-3}$  and  $[\text{HO}_2]_0 = 1.0 \times 10^{12} \text{ molecule cm}^{-3}$  as compared to the background signal (■) obtained with the  $\text{HO}_2$  source turned off. Linear least squares fits to both data sets are plotted as solid lines to guide the eye, and the 95% confidence interval for the background data is plotted as dashed lines.

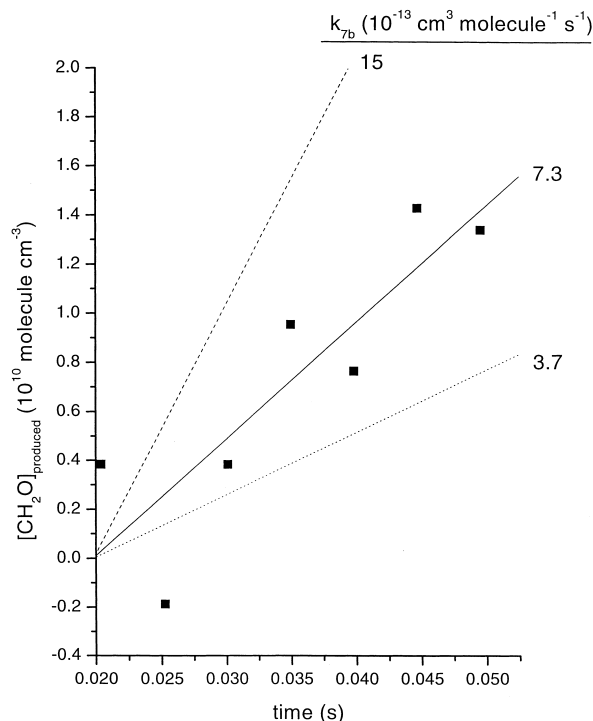
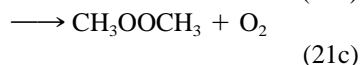
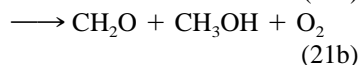
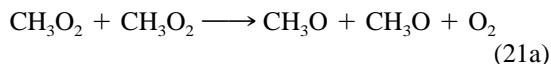


**Figure 6** Sensitivity of fitted value of  $k_{7b}$  to the data given in Figure 5.

calibrated initial concentrations of  $\text{CH}_3\text{O}_2$  and  $\text{HO}_2$  and the reactions listed in Table I. Although the agreement between the experimental data and the model curve appears excellent, the lack of a formal calibration for  $\text{CH}_3\text{OOH}$  precludes the quantitative determination of the rate constant for this branching channel ( $k_{7a}$ ). However, Figure 4 does provide confirming evidence that the  $\text{CH}_3\text{OOH}$ -producing branching channel is in fact the major product pathway for the  $\text{CH}_3\text{O}_2 + \text{HO}_2$  reaction. We chose not to pursue the quantitative determination of  $k_{7a}$  because the partitioning between two competing channels is best determined by measurements of the minor channel ( $k_{7b}$ , in the case of  $\text{CH}_3\text{O}_2 + \text{HO}_2$ ), which is described in the following paragraph.

The major complication in the rate-constant determination for the  $\text{CH}_2\text{O}$  producing channel ( $k_{7b}$ ) is the  $\text{CH}_2\text{O}$ -producing side reaction resulting from the self-reaction of  $\text{CH}_3\text{O}_2$ :



( $k_{21} = 4.7 \times 10^{-13} \text{ cm}^3 \text{ molecule}^{-1} \text{ s}^{-1}$ ) [14]. Note that

$\text{CH}_2\text{O}$  is directly produced via reaction (21b) and indirectly produced via reaction (21a) in the presence of oxygen by coupling to reaction (11).



At 298 K, the JPL recommendation for reaction (21) indicates the following branching ratios for channels a, b, and c, respectively: 0.3, 0.6, and 0.1 [14]. Therefore, 60% of the total  $\text{CH}_3\text{O}_2 + \text{CH}_3\text{O}_2$  reactive events lead to  $\text{CH}_2\text{O}$ ; in the presence of sufficient  $\text{O}_2$ , the fraction increases to 90% (also note that channel 21a produces two  $\text{CH}_2\text{O}$  molecules per reactive event, while channel 21b produces only one). For our experimental conditions ( $[\text{O}_2] \sim 3.0 \times 10^{16} \text{ molecule cm}^{-3}$ ), the  $\text{CH}_2\text{O}$ -producing fraction is predicted to be near the limiting 90% value. Because main flow concentrations of  $\text{CH}_3\text{O}_2$  are low ( $< 1.0 \times 10^{12} \text{ molecule cm}^{-3}$ ) compared to the overall rate constant, it might be expected that reaction (21) would lead to small  $\text{CH}_2\text{O}$  background levels. However,  $\text{CH}_3\text{O}_2$  concentrations are about 15 times higher in the sidearm of the flow tube where it is produced, thus increasing the rate of the self-reactions given above before they enter the main flow tube. In fact, the sidearm reaction time was optimized (by varying the position in the sidearm where the F atoms were injected) to achieve the most favorable conditions (i.e., the largest  $\text{CH}_3\text{O}_2/\text{CH}_2\text{O}$  ratio possible). Using the relevant concentrations and times for  $\text{CH}_3\text{O}_2$  self-reaction in the sidearm and a kinetic model incorporating the reactions given above, we estimate that for the largest main flow-tube concentrations of  $[\text{CH}_3\text{O}_2]_0$  used ( $1.0 \times 10^{12} \text{ molecule cm}^{-3}$ ), a “background” main flow-tube concentration of  $[\text{CH}_2\text{O}] \sim 1.5 \times 10^{11} \text{ molecule cm}^{-3}$  should be observed. This background source of  $\text{CH}_2\text{O}$  is a constant with respect to the kinetics data collected (the  $\text{CH}_3\text{O}_2$  source is spatially fixed, and thus all reactions involving species originating from it have the same total reaction time regardless of the  $\text{HO}_2$  injector position). Since none of the  $\text{CH}_2\text{O}$ -producing reactions listed in Table I depends on the presence of  $\text{HO}_2$ , we expect that any  $\text{CH}_2\text{O}$  produced from side reactions should not depend on the  $\text{HO}_2$  injector position. However, it is possible that the additional  $\text{O}_2$  added to the flow system through the  $\text{HO}_2$  injector could lead to additional production of  $\text{CH}_2\text{O}$  via reactions (21a) and (11) that would appear to depend on the position of the  $\text{HO}_2$  injector. In Figure 5, the raw  $\text{CH}_2\text{O}$  signal vs. injector distance data is presented for two experiments: The data depicted as circle symbols was collected with the  $\text{HO}_2$  source on, and the data depicted as square symbols was collected with the  $\text{HO}_2$  source off (all gases flowing, but the microwave discharge



was turned off). It is apparent from these experiments that no additional CH<sub>2</sub>O is formed by the introduction of gases used to synthesize HO<sub>2</sub> (helium, hydrogen, and oxygen). It is also apparent that the CH<sub>2</sub>O produced with the HO<sub>2</sub> source operating is statistically significant, as the CH<sub>2</sub>O signal is observed rising above the 95% confidence interval for the CH<sub>2</sub>O time-dependent profile obtained with the HO<sub>2</sub> source turned off. Using the CH<sub>2</sub>O calibration factor and the total CH<sub>2</sub>O signal observed for the experiments depicted in Figure 5, a background CH<sub>2</sub>O level of about  $1.7 \times 10^{11}$  molecule cm<sup>-3</sup> is calculated. As discussed above, this background level is consistent with kinetic model results for the production of CH<sub>2</sub>O via CH<sub>3</sub>O<sub>2</sub> self-reaction chemistry. In summary, despite the fact that a relatively large CH<sub>2</sub>O background signal is observed (which is consistent with kinetic modeling of the CH<sub>3</sub>O<sub>2</sub> self-reaction chemistry occurring in the side-arm reactor), we are able to observe CH<sub>2</sub>O production as a function of HO<sub>2</sub> contact time that can be positively attributed to the CH<sub>3</sub>O<sub>2</sub> + HO<sub>2</sub> reaction.

Figure 6 shows the CH<sub>2</sub>O production observed (squares) for the reaction conditions given in Figure 5, with a solid line fit through the data to determine the rate of CH<sub>2</sub>O production, which is used in the fitting process to determine  $k_{7b}$ . The value of  $k_{7b}$  was fitted by using a kinetic model that included the reactions and rate parameters given in Table I and the

experimental initial concentrations of CH<sub>3</sub>O<sub>2</sub>, HO<sub>2</sub>, and O<sub>2</sub> to calculate the rate of CH<sub>2</sub>O production for comparison to the experimentally determined rate of CH<sub>2</sub>O production. The value of  $k_{7a}$  in the fitting process was constrained by the relationship  $k_{7a} = k_7 - k_{7b}$ , where  $k_7$  was calculated from the JPL-recommended Arrhenius parameters [14]. In Figure 6, along with fitted value for  $k_{7b}$  (solid line),  $k_{7b}$  values that are a factor of 2 higher (dashed line) and a factor of 2 lower (dotted line) are used to predict CH<sub>2</sub>O profiles to illustrate the sensitivity of the fitted value of  $k_{7b}$  to the actual CH<sub>2</sub>O profile observed. It is apparent from this plot and the statistical uncertainties reported in Table II that the fitted  $k_{7b}$  values are determined to a precision of about 50%.

The experiments were carried out at several different [CH<sub>3</sub>O<sub>2</sub>]<sub>0</sub> and [HO<sub>2</sub>]<sub>0</sub> concentrations, which provide a test of consistency for the kinetic model and the method of data analysis. Table II lists the experimental conditions and fitted  $k_{7b}$  values (and associated branching ratios) for all experiments performed. In particular, several different [CH<sub>3</sub>O<sub>2</sub>]<sub>0</sub> values (at nearly fixed HO<sub>2</sub> concentrations) were used to test the consistency of the  $k_{7b}$  determination method. Figure 7 shows that very similar  $k_{7b}$  values were obtained for these experiments with differing initial CH<sub>3</sub>O<sub>2</sub> concentrations. Although this test does not rule out other systematic errors in the fitting of  $k_{7b}$  (such as HO<sub>2</sub> calibration errors or

**Table II** Branching Ratio Data for the CH<sub>3</sub>O<sub>2</sub> + HO<sub>2</sub> → CH<sub>2</sub>O + H<sub>2</sub>O + O<sub>2</sub> Reaction at 100 Torr Pressure

<i>T</i> (K)	[CH <sub>3</sub> O <sub>2</sub> ] <sub>0</sub> (10 <sup>10</sup> molecule cm <sup>-3</sup> )	[HO <sub>2</sub> ] <sub>0</sub> (10 <sup>10</sup> molecule cm <sup>-3</sup> )	$k_{7b}$ (and 1σ error) (10 <sup>-14</sup> cm <sup>3</sup> molecule <sup>-1</sup> s <sup>-1</sup> )	Branching Ratio $k_{7b}/(k_{7a} + k_{7b})$
298	39	125	56 ± 22	0.10
298	38	100	56 ± 39	0.10
298	92	100	45 ± 39	0.08
298	63	100	73 ± 28	0.13
298	42	115	67 ± 34	0.12
273	80	100	57 ± 50	0.08
273	88	100	71 ± 71	0.10
263	80	76	104 ± 40	0.13
263	80	76	104 ± 32	0.13
253	77	139	180 ± 54	0.20
253	77	139	144 ± 63	0.16
253	77	139	144 ± 63	0.16
253	77	139	135 ± 36	0.15
243	82	140	150 ± 40	0.15
243	82	140	150 ± 30	0.15
243	82	140	120 ± 50	0.12
237	60	139	231 ± 55	0.21
230	48	79	431 ± 130	0.35
230	50	79	357 ± 86	0.29
218	52	79	492 ± 130	0.33
218	52	79	447 ± 270	0.30

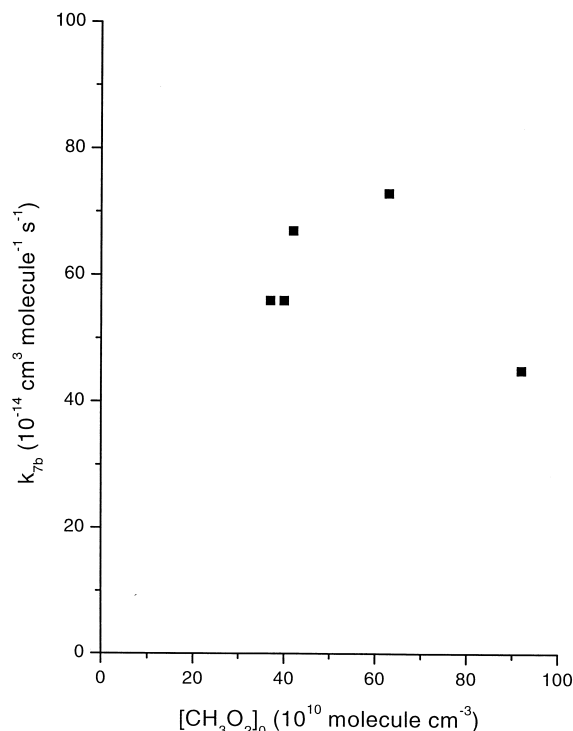


**Figure 7** Dependence of the fitted  $\text{CH}_3\text{O}_2 + \text{HO}_2 \rightarrow \text{CH}_2\text{O} + \text{H}_2\text{O} + \text{O}_2$  branching channel rate constant on initial  $\text{CH}_3\text{O}_2$  concentration.

unknown sources of  $\text{CH}_2\text{O}$  originating from species produced in the  $\text{HO}_2$  injector), it does suggest that the  $\text{CH}_3\text{O}_2$  calibration is not subject to large systematic error, and thus the fitted values of  $k_{7b}$  are fairly reliable from the point of view of the modeled  $\text{CH}_3\text{O}_2$  chemistry. The error given in Table II represents the statistical uncertainty determined in the fitting process and does not include contributions from systematic error. We have previously estimated that the largest source of systematic error in these types of experiments results from the titration/calibration methods used for  $\text{HO}_2$  and  $\text{CH}_3\text{O}_2$  [4]. We estimate that this error is on the order of  $\pm 15\%$  ( $1\sigma$ ) for these species as well as

for the  $\text{CH}_2\text{O}$  calibration method. In addition, uncertainties in the rate constants used in the fitting process can also introduce systematic error to the determination of  $k_{7b}$  (in particular, the uncertainty in  $k_7$ , which propagates nearly linearly into the value of  $k_{7b}$ ). There is also some uncertainty in the determination of absolute reaction time from the flow velocity and distance from the injector tip to the mass spectrometer sampling aperture. However, this uncertainty is probably fairly low since the flow velocity depends directly on the accuracy of the mass flow meters (calibrated to at least 5% accuracy) and the distance is uncertain to less than 1 cm (the distance between the ionization region and the mass spectrometer aperture), or about 2% of the longest reaction time. Nonetheless, it is clear that relatively large systematic errors (as much as 50%,  $1\sigma$ ) are potentially present in our fitted values for  $k_{7b}$ .

Based on our five fitted  $k_{7b}$  values at 298 K and 100 Torr, we calculate a value (and  $1\sigma$  statistical uncertainty) for the branching ratio  $[k_{7b}/(k_{7a} + k_{7b})]$  of  $0.11 \pm 0.02$ . Table III lists the product monitored, experimental conditions, and inferred values for the branching ratio from the previous indirect ( $\text{CH}_2\text{O}$  is not directly detected) studies as well as the present direct ( $\text{CH}_2\text{O}$  is directly detected) one. The kinetics study of Moortgat et al. [9] involved the simultaneous monitoring of peroxy radicals and  $\text{CH}_3\text{OOH}$  at 298 K and 700 torr, which allowed the determination of an overall rate constant ( $4.8 \times 10^{-12} \text{ cm}^3 \text{ molecule}^{-1} \text{ s}^{-1}$ ; compared to the current JPL recommended value of  $5.6 \times 10^{-12} \text{ cm}^3 \text{ molecule}^{-1} \text{ s}^{-1}$  used in this work) as well as a specific  $\text{CH}_3\text{OOH}$ -producing rate constant ( $3.5 \times 10^{-12} \text{ cm}^3 \text{ molecule}^{-1} \text{ s}^{-1}$ ). From these rate constants, a  $\text{CH}_2\text{O}$ -producing branching ratio of 0.27 may be inferred. In the work of Jenkin et al. [8],  $\text{CD}_3\text{O}_2$  was used as a reactant and the production of HDO was followed at 298 K and 11 torr. The branching ratio determined by Jenkin et al. was determined in a manner similar to the present work; the rate constant for HDO (formed along with  $\text{CD}_2\text{O}$  and  $\text{O}_2$ ) pro-

**Table III** Comparison of Branching Ratio Determinations for the  $\text{CH}_3\text{O}_2 + \text{HO}_2$  Reaction

Study	Product Monitored	Temperature (K)	Pressure (Torr)	$k_{7b}/(k_{7a} + k_{7b})$
Moortgat <i>et al.</i> [9]	$\text{CH}_3\text{OOH}$	298	700	0.27
Jenkin <i>et al.</i> [8]	HDO <sup>a</sup>	298	11	0.40
Wallington [16]	$\text{CH}_3\text{OOH}$	298	15–700	$0.08 \pm 0.05$
This work	$\text{CH}_2\text{O}$	298	100	$0.11 \pm 0.02$
This work	$\text{CH}_2\text{O}$	218–298	100	$\left[1 + e^{\left(\frac{-1160}{T} + 6.21\right)}\right]^{-1}$

<sup>a</sup> From measurements of the reaction  $\text{CD}_3\text{O}_2 + \text{HO}_2 \rightarrow \text{CD}_2\text{O} + \text{HDO} + \text{O}_2$ .

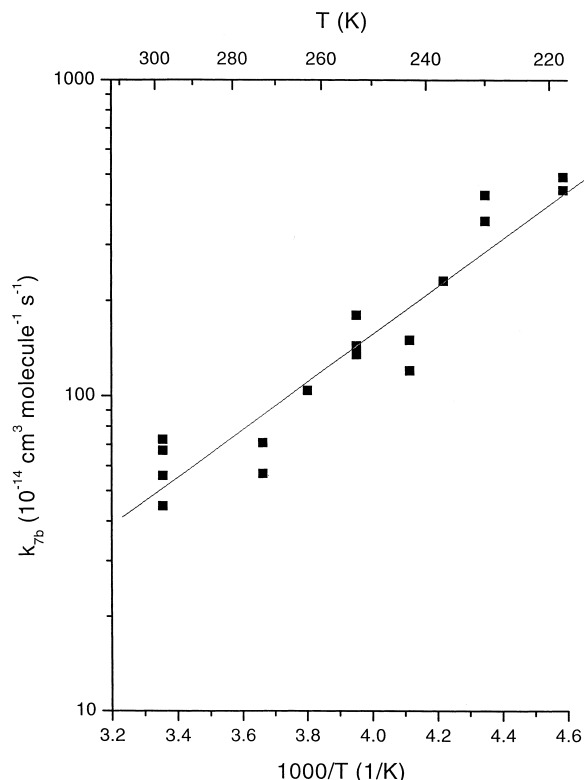


**Figure 8** Arrhenius plot of the temperature dependence of the rate constant at 100 Torr pressure of the  $\text{CH}_3\text{O}_2 + \text{HO}_2 \rightarrow \text{CH}_2\text{O} + \text{H}_2\text{O} + \text{O}_2$  branching channel (■: actual data; —: fit to data).

duction was directly determined, and the branching ratio was determined by dividing this value by their value for the overall rate constant ( $5.4 \times 10^{-12} \text{ cm}^3 \text{ molecule}^{-1} \text{ s}^{-1}$ ). As Jenkin et al. point out, their  $\text{CD}_2\text{O}$ -producing branching ratio result of 0.40 for  $\text{CD}_3\text{O}_2$  must be interpreted with care, as kinetic isotope effects are likely to make the  $\text{CH}_2\text{O}$ -producing results for  $\text{CH}_3\text{O}_2$  somewhat different. Wallington [16] determined the fraction of  $\text{CH}_3\text{OOH}$  produced from the  $\text{CH}_3\text{O}_2 + \text{HO}_2$  reaction at 298 K and several pressures by performing a carbon mass balance analysis. From the “missing carbon,” a  $\text{CH}_2\text{O}$ -producing branching ratio of 0.08 may be inferred. Our direct result is in excellent agreement with the inferred result of Wallington [16], while it is substantially lower than the values inferred from the work of Moortgat et al. [9] and Jenkin et al. [8].

### Temperature Dependence of the CH<sub>2</sub>O Branching Channel Rate-Constant Determination

In order to establish a set of branching ratio values for the whole range of tropospherically relevant temper-

atures, we performed several measurements of  $k_{7b}$  at temperatures between 218 and 298 K in order to determine the temperature dependence of the  $\text{CH}_2\text{O}$  branching channel. From the data listed in Table II and plotted in Figure 8, we obtained the following Arrhenius expression (with  $1\sigma$  statistical uncertainties):  $k_{7b}(T) = 1.6_{-0.7}^{+1.0} \times 10^{-15} \times \exp[(1730 \pm 130)/T] \text{ cm}^3 \text{ molecule}^{-1} \text{ s}^{-1}$ . It is clear from the data and the fitted Arrhenius expression that both  $k_{7b}$  and the branching ratio ( $k_{7b}$  increases even more quickly than  $k_7$  as the temperature decreases) show a steep negative temperature dependence:  $k_7$  increases by a factor of  $\sim 7$ , and the branching ratio increases by a factor of  $\sim 3$  as the temperature is decreased from 298 to 218 K. The negative temperature dependence of  $k_7$  is consistent with the formation of a reactive intermediate. Figure 9 depicts a potential mechanism for reaction (7b) that is based on a six-membered ring intermediate structure that rearranges to produce the observed products. The more dramatic negative temperature dependence of  $k_{7b}$  suggests that the  $\text{CH}_2\text{O}$ -producing product channel is even more dependent on efficient thermal stabilization of the intermediate than is the  $\text{CH}_3\text{OOH}$ -producing channel. Given the very specific intermediate geometry required for the  $\text{CH}_2\text{O}$ -forming mechanism shown in Figure 9, the steep negative temperature dependence of  $k_{7b}$  seems consistent with the proposed mechanism.

Since the  $\text{CH}_3\text{O}_2 + \text{CH}_3\text{O}_2$  reaction has similar product channels to the  $\text{CH}_3\text{O}_2 + \text{HO}_2$  reaction, it is of interest to compare the temperature dependences of the branching ratios for these reactions. There have been several previous studies of the temperature dependence of the branching channels for the  $\text{CH}_3\text{O}_2 + \text{CH}_3\text{O}_2$  reaction (for a review, see ref. [25]). Although other workers have reported the existence of a  $\text{CH}_3\text{OOCH}_3$ -producing channel (reaction (21c)), the most recent work of Tyndall et al. indicates no evidence for that channel (an upper limit of 6% is estimated) [26]. Accordingly, one can consider the temperature dependence of just the two major product channels for the  $\text{CH}_3\text{O}_2 + \text{CH}_3\text{O}_2$  reaction:

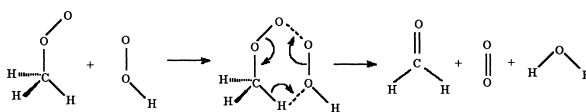
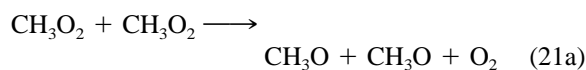


**Figure 9** Proposed mechanism for the  $\text{CH}_3\text{O}_2 + \text{HO}_2 \rightarrow \text{CH}_2\text{O} + \text{H}_2\text{O} + \text{O}_2$  branching channel.

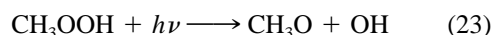
In these experiments, a branching ratio, defined as  $\alpha = [k_{21a}/(k_{21a} + k_{21b})]$ , was measured as a function of temperature. In order to allow an Arrhenius analysis, the branching ratio data were converted to the ratio defined as  $\beta = k_{21a}/k_{21b}$ . In order to generalize this ratio to the  $\text{CH}_3\text{O}_2 + \text{HO}_2$  analysis as well, this term can be thought of as the ratio of the “direct”  $\text{O}_2$  elimination channel to the “indirect” (hydrogen transfer)  $\text{O}_2$  elimination channel. For both  $\text{CH}_3\text{O}_2 + \text{CH}_3\text{O}_2$  and  $\text{CH}_3\text{O}_2 + \text{HO}_2$ , the “indirect” channel produces  $\text{CH}_2\text{O}$ . Based on all available data, Lightfoot et al. obtained the following Arrhenius-type expression for  $\text{CH}_3\text{O}_2 + \text{CH}_3\text{O}_2$ :  $\ln \beta = 3.22 - 1165/T$  [25]. In order to directly compare the temperature dependence of the branching ratio obtained for the  $\text{CH}_3\text{O}_2 + \text{HO}_2$  reaction with that for  $\text{CH}_3\text{O}_2 + \text{CH}_3\text{O}_2$ , we also recast our data in terms of  $\beta (= k_{7a}/k_{7b}$  for  $\text{CH}_3\text{O}_2 + \text{HO}_2$ ) and obtained the following Arrhenius-type expression:  $\ln \beta = 6.21 - 1160/T$ . These expressions reveal remarkable agreement in the temperature dependence of the  $\text{CH}_2\text{O}$  producing channels for the  $\text{CH}_3\text{O}_2 + \text{CH}_3\text{O}_2$  and  $\text{CH}_3\text{O}_2 + \text{HO}_2$  reactions. The  $\text{C}_2\text{H}_5\text{O}_2 + \text{C}_2\text{H}_5\text{O}_2$  reaction proceeds through analogous product channels to produce  $\text{CH}_3\text{CHO}$ , albeit at smaller branching ratio at 298 K (0.3 for the direct  $\text{CH}_3\text{CHO}$ -producing channel) as well as a less steep negative temperature dependence ( $\ln \beta = 2.32 - 533/T$ ) than for  $\text{CH}_3\text{O}_2 + \text{CH}_3\text{O}_2$  [25]. Current experimental evidence obtained at 298 K seems to indicate that the  $\text{C}_2\text{H}_5\text{O}_2 + \text{HO}_2$  reaction does not have a significant  $\text{CH}_3\text{CHO}$ -producing channel [27]. However, our finding that the  $\text{CH}_2\text{O}$ -producing channels for  $\text{CH}_3\text{O}_2 + \text{CH}_3\text{O}_2$  and  $\text{CH}_3\text{O}_2 + \text{HO}_2$  have similarly strong negative temperature dependences may indicate that the  $\text{C}_2\text{H}_5\text{O}_2 + \text{HO}_2$  reaction has the potential to have a significant  $\text{CH}_3\text{CHO}$ -producing channel at low temperatures. Finally, from our definition of  $\beta = k_{7a}/k_{7b}$ , we can derive a convenient term for the temperature dependence of the  $\text{CH}_2\text{O}$  branching ratio for the  $\text{CH}_3\text{O}_2 + \text{HO}_2$  reaction:

$$k_{7b}/(k_{7a} + k_{7b}) = 1/(1 + \beta) = [1 + e^{(-1160/T + 6.21)}]^{-1} \quad (22)$$

### Atmospheric Significance of $\text{CH}_2\text{O}$ Production from $\text{CH}_3\text{O}_2 + \text{HO}_2$ Reaction

As we have established that the  $\text{CH}_3\text{O}_2 + \text{HO}_2$  reaction possesses a significant  $\text{CH}_2\text{O}$ -producing branching channel (which increases in significance as the temperature is lowered), it is of interest to consider how this result may impact atmospheric models, which generally assume a branching ratio of zero for the  $\text{CH}_2\text{O}$ -producing channel. Because high  $\text{NO}_x$  levels

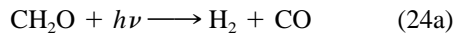
circumvent  $\text{CH}_2\text{O}$  production via either  $\text{CH}_3\text{O}_2 + \text{HO}_2$  pathway [reactions (4a) and (11) instead determine the rates of  $\text{CH}_2\text{O}$  production], we expect that reaction (7b) is of minor significance in highly polluted environments. However, we propose two potential impacts on the prediction accuracy of atmospheric models in environments (relatively low  $\text{NO}_x$ ) where significant direct  $\text{CH}_2\text{O}$  production via reaction (7b) can occur. The atmospheric fate of  $\text{CH}_3\text{OOH}$  (the main channel product of the  $\text{CH}_3\text{O}_2 + \text{HO}_2$  reaction) is also the eventual formation of  $\text{CH}_2\text{O}$ :



An obvious potential effect is that if the reaction (7b) pathway is faster than the reaction (7a/23/11) pathway currently used in atmospheric models, one would expect that observed  $\text{CH}_2\text{O}$  levels might be higher than predicted. From the atmospheric lifetimes for the relevant species (derived using background  $\text{NO}_x$  levels) presented in Lawrence et al., it does appear that the reaction (7b) pathway ( $\sim$ hours) should be significantly faster than the reaction (7a/23/11) pathway ( $\sim$ days), which is limited by the relatively long lifetime of  $\text{CH}_3\text{OOH}$  against photolysis [28]. In fact, Ayers et al. had earlier found that observed  $\text{CH}_2\text{O}$  levels at Cape Grim, Tasmania (a location characterized by very low  $\text{NO}_x$  levels), were underpredicted by atmospheric models, which assumed a  $k_{7b}$  value of zero [17]. However, Ayers et al. found that a branching ratio of 0.40 was required to reconcile the observed  $\text{CH}_2\text{O}$  levels with the model results, a value significantly larger than the one reported here. More recently, Weller et al. reported the results of  $\text{CH}_2\text{O}$  measurements in the marine boundary layer of the Atlantic and came to a similar conclusion: Observed  $\text{CH}_2\text{O}$  levels were greater than the predictions from a photochemical model using a  $k_{7b}$  value of zero [18]. Following the earlier work of Ayers et al., Weller et al. added reaction (7b) to their model (again with a branching ratio of 0.40) and found that the predicted  $\text{CH}_2\text{O}$  concentrations were in closer (although not full) agreement with their atmospheric observations. Therefore, although our present study presents evidence for a significant  $\text{CH}_2\text{O}$ -forming product channel from the  $\text{CH}_3\text{O}_2 + \text{HO}_2$  reaction, it appears that the  $k_{7b}$  value determined here will not fully reconcile model predictions and atmospheric observations of  $\text{CH}_2\text{O}$ .

A less obvious effect of nonnegligible  $\text{CH}_2\text{O}$  production via reaction (7b) might involve a modification of the efficiency of  $\text{HO}_x$  cycling.  $\text{CH}_2\text{O}$  itself has only

a short atmospheric lifetime against photolysis (~hours) [28]:



with the two branching channels being roughly equal for overhead solar conditions [29]. Both products of reaction (24b) lead to the formation of HO<sub>2</sub>:



Therefore, the existence of a significant CH<sub>2</sub>O-producing channel for the CH<sub>3</sub>O<sub>2</sub> + HO<sub>2</sub> reaction could lead to faster HO<sub>x</sub> regeneration simply because CH<sub>2</sub>O is produced faster via reaction (7b) than via reactions (7a/23/11). This effect may be a contributing factor in the search for an answer to the observation that observed HO<sub>x</sub> levels in the upper troposphere are greater than those predicted by current atmospheric models (which assume a value of zero for  $k_{7b}$ ) [5].

## CONCLUSIONS

The results presented here represent the first direct measurement of the CH<sub>2</sub>O-producing channel of the CH<sub>3</sub>O<sub>2</sub> + HO<sub>2</sub> reaction, as well as the first product-specific temperature-dependence study of any kind for this reaction. The kinetics of the reactant CH<sub>3</sub>O<sub>2</sub> and the main branching channel product CH<sub>3</sub>OOH were also monitored and found to be consistent with JPL recommendation for the overall rate constant [14]. This study indicates the CH<sub>3</sub>O<sub>2</sub> + HO<sub>2</sub> reaction should be a significant source of CH<sub>2</sub>O in the troposphere, as the branching ratio [ $k_{7b}/(k_{7a} + k_{7b})$ ] at 100 Torr was found to be 0.11 at 298 K and increased to 0.31 as the temperature was lowered to 218 K. This work should help improve the kinetics database for methane oxidation chemistry by placing more stringent constraints on CH<sub>2</sub>O and HO<sub>x</sub> formation and destruction rates. In particular, these findings may help explain larger-than-predicted (by models which assume a  $k_{7b}$  value of zero) CH<sub>2</sub>O observations in the clean troposphere, as well as larger-than-predicted HO<sub>x</sub> levels in the upper troposphere.

This research was funded by grants from the National Science Foundation (ATM-9874752), the Towsley Foundation,

the Camille and Henry Dreyfus Foundation, the American Chemical Society–Petroleum Research Fund, and Research Corporation.

## BIBLIOGRAPHY

1. Finlayson-Pitts, B. J.; Pitts, J. N. *Chemistry of the Upper and Lower Atmosphere*; Academic Press: San Diego, 1999.
2. Bertman, S. B.; Roberts, J. M.; Parrish, D. D.; Buhr, M. P.; Goldan, P. D.; Kuster, W. C.; Fehsenfeld, F. C.; Montzka, S. A.; Westberg, H. J. *Geophys Res* 1995, 100, 22805.
3. Flocke, F.; Atlas, E.; Madronich, S.; Schauffler, S. M.; Aikin, K.; Margitan, J. J.; Bui, T. P. *Geophys Res Lett* 1998, 25, 1891.
4. Scholtens, K. W.; Messer, B. M.; Cappa, C. D.; Elrod, M. J. *J Phys Chem A* 1999, 103, 4378.
5. Wennberg, P. O.; Hanisco, T. F.; Jaeglé, L.; Jacob, D. J.; Hints, E. J.; Lanzendorf, E. J.; Anderson, J. G.; Gao, R.; Keim, E. R.; Donnelly, S. G.; Negro, L. A.; Fahey, D. W.; McKeen, S. A.; Salawitch, R. J.; Webster, C. R.; May, R. D.; Herman, R. L.; Proffitt, M. H.; Margitan, J. J.; Atlas, E. L.; Schauffler, S. M.; Flocke, F.; McElroy, C. T.; Bui, T. P. *Science* 1998, 279, 49.
6. Cox, R. A.; Tyndall, G. S. *Chem Phys Lett* 1979, 65, 357.
7. Cox, R. A.; Tyndall, G. S. *J Chem Soc, Faraday Trans 2* 1980, 76, 153.
8. Jenkin, M. E.; Cox, R. A.; Hayman, G. D.; Whyte, L. J. *J Chem Soc, Faraday Trans 2* 1988, 84, 913.
9. Moortgat, G. K.; Cox, R. A.; Schuster, G.; Burrows, J. P.; Tyndall, G. S. *J Chem Soc, Faraday Trans 2* 1989, 85, 809.
10. McAdam, K.; Veyret, B.; Lesclaux, R. *Chem Phys Lett* 1987, 133, 39.
11. Kurylo, M. J.; Dagaut, P.; Wallington, T. J.; Neuman, D. M. *Chem Phys Lett* 1987, 139, 513.
12. Dagaut, P.; Wallington, T. J.; Kurylo, M. J. *J Phys Chem* 1988, 92, 3833.
13. Lightfoot, P. D.; Veyret, B.; Lesclaux, R. *J Phys Chem* 1990, 94, 708.
14. DeMore, W. B.; Sander, S. P.; Howard, C. J.; Ravishankara, A. R.; Golden, D. M.; Kolb, C. E.; Hampson, R. F.; Kurylo, M. J.; Molina, M. J. *Chemical Kinetics and Photochemical Data for Use in Stratospheric Modeling* JPL Publication 97-4, Jet Propulsion Laboratory: Pasadena, California, 1997.
15. Kan, C. S.; Calvert, J. G.; Shaw, J. H. *J Phys Chem* 1980, 84, 3411.
16. Wallington, T. J. *J Chem Soc, Faraday Trans* 1991, 87, 2379.
17. Ayers, G. P.; Gillett, R. W.; Granek, H.; de Serves, C.; Cox, R. A. *Geophys Res Lett* 1997, 24, 401.
18. Weller, R.; Schrems, O.; Boddenberg, A.; Gab, S.; Gautrois, M. *J Geophys Res* 2000, 105, 14401.

19. Seeley, J. V.; Jayne, J. T.; Molina, M. J. *Int J Chem Kinet* 1993, 25, 571.
20. Ranschaert, D. L.; Schneider, N. J.; Elrod, M. J. *J Phys Chem A* 2000, 104, 4449.
21. Elrod, M. J.; Meads, R. F.; Lipson, J. B.; Seeley, J. V.; Molina, M. J. *J Phys Chem* 1996, 100, 5808.
22. Midey, A. J.; Arnold, S. T.; Viggiano, A. A. *J Phys Chem A* 2000, 104, 2706.
23. Huey, L. G.; Hanson, D. R.; Howard, C. J. *J Phys Chem* 1995, 99, 5001.
24. Messer, B. M.; Stielstra, D. E.; Cappa, C. D.; Scholtens, K. W.; Elrod, M. J. *Int J Mass Spectrom* 2000, 197, 219.
25. Lightfoot, P. D.; Cox, R. D.; Crowley, J. N.; Destriau, G. D.; Hayman, G. D.; Jenkin, M. E.; Moortgat, G. K.; Zabel, T. *Atmos Env* 1992, 26A, 1805.
26. Tyndall, G. S.; Wallington, T. J.; Ball, J. C. *J Phys Chem A* 1998, 102, 2547.
27. Wallington, T. J.; Japar, S. M. *Chem Phys Lett* 1990, 166, 495.
28. Lawrence, M. G.; Crutzen, P. J.; Rasch, P. J.; Eaton, B. E.; Mahowald, N. M. *J Geophys Res Atmos* 1999, 104, 26245.
29. Seinfeld, J. H.; Pandis, S. N. *Atmospheric Chemistry and Physics*; John Wiley and Sons, Inc.: New York, 1998.